

# Experimental and numerical studies for buckling and collapse behaviors of a cracked thin steel panel subjected to sequential tensile and compressive loading

Septia Hardy Sujatanti<sup>a,b</sup>, Satoyuki Tanaka<sup>a,\*</sup>,  
Shuhei Shinkawa<sup>a</sup>, Yu Setoyama<sup>c</sup>, Daisuke Yanagihara<sup>d</sup>

<sup>a</sup>*Graduate School of Advanced Science and Engineering, Hiroshima University, Japan, e-mail: satoyuki@hiroshima-u.ac.jp, m176289@hiroshima-u.ac.jp*

<sup>b</sup>*Department of Naval Architecture, Institut Teknologi Sepuluh Nopember, Indonesia, e-mail: septia.rahmadianto@gmail.com*

<sup>c</sup>*Fujitsu Kyushu Systems Limited, Japan, e-mail: ysetoyama@fujitsu.com*

<sup>d</sup>*Graduate School of Engineering, Kyushu University, Japan, e-mail: yanagihara@nams.kyushu-u.ac.jp*

---

## Abstract

The buckling and collapse behaviors of a cracked thin steel panel subjected to sequential tensile and compressive loading were investigated. An experimental apparatus was developed. Three different test specimens were employed, *i.e.*, an intact panel and cracked panels with different crack lengths. The load-displacement curve and crack opening displacement (COD) were measured during the loading. The experimental results were examined via finite element (FE) computation. The results revealed that the developed experimental apparatus is quite suitable for investigating the buckling and collapse behaviors. Furthermore, the maximum tensile load, ultimate strength and local deformation around the crack were well simulated by the FE computation. The presence of the crack and length of the crack were strongly affected to the buckling and collapse behaviors.

*Keywords:* Cracked Steel Panel, Buckling, Ultimate Strength, Experimental Study, Finite Element Computation

---

---

\*Corresponding author

## 1. Introduction

Ship structural components, *i.e.*, hull girders [1-3] and stiffened panel structures [4-7] are mainly composed of steel structural members such as beams, stiffeners and panels. Crack-like defects may occur during the service period due to various factors, *e.g.*, corrosion, fatigue and local buckling. These defects are preferentially generated in welded joints, structural discontinuities and stress concentration parts. Damage to the structural components affects the tensile, bending, buckling and ultimate strengths. When a cyclic load is applied to the components, small defects will develop and finally cause large-scale damage to the structures. Therefore, mechanical evaluation of the cracked structural components is essential for ensuring the structural safety and integrity of these components. Fracture mechanics represents one of the main methodologies for evaluating fatigue and fracture problems [8-15]. However, fracture assessment of thin-walled structures is still in its infancy and includes complex problems, such as geometrical nonlinearity, buckling, in-plane/out-of-plane mixed-mode fracture and crack propagation.

The finite element method (FEM) has been used to investigate the mechanical characteristics of cracked panel structures. Furthermore, the buckling and collapse behaviors of cracked panels under compressive loads were analyzed [16-18]. Cracked panels under tensile loading were investigated and the results revealed that local buckling occurs around the crack due to Poisson's ratio effect [19,20]. Sih and Lee [21] assessed the mechanical behavior of cracked panels under tension and compression and the deformation mode was investigated. Brighenti [22-24] analyzed cracked thin panels subjected to tensile and compressive loads and performed a sensitivity analysis on the buckling problems. Additionally, the collapse and ultimate strength behaviors of crack damaged stiffened panels under compressive loads were discussed from the viewpoint of establishing a damage-tolerant procedure for the stiffened structure under compression loading [25-27]. Yanagihara *et al.* conducted collapse analysis of a cracked stiffened panel by employing shell FEs that consider the crack contact effect [28-29]. Babazadeh and Khedmati [30] summarized the collapse analysis results obtained for cracked ship structural elements and systems. Several factors influencing the ultimate strength (such as the crack length, crack location, panel thickness, aspect ratio and boundary condition (BC)) were discussed. Moreover, the authors have considered several shell buckling [31-35] and shell fracture problems [36-40] by using a meshfree method to explore the mechanical characteristics of cracked

shell structures.

Additionally, experimental studies of cracked panels have been conducted. The ultimate strength of cracked elements subjected to axial compressive or tensile loads was determined via experimental and numerical methods [41,42]. The residual ultimate strength due to crack damage of panel elements was investigated by varying the crack position and crack length. The buckling failure of a cracked panel under a compressive load was investigated by means of experiments, where the panel thickness and aspect ratio were varied [43]. Moreover, the critical local buckling induced by the applied tensile loading of a cracked panel was investigated via experiment [44]. Shi *et al.* [45] have evaluated the behavior of a cracked stiffened panel under compression through experiments.

Ship structural members experience repetitive tensile and compressive stresses under several internal and external loads. As a result, these structures are prone to induce fatigue and fracture damage. A tensile load is applied to a cracked steel panel, the crack opens gradually and the crack tip is blunted due to yielding. In addition, a compressive load is applied to the panel, the crack is closed and buckling occurs. The mechanical behaviors will be complex compared with those of the monotonic tensile or compressive load cases. In a previous study, the authors investigated the buckling and collapse behaviors of a cracked rectangular panel subjected to sequential tensile and compressive loading [46]. When the gap between the crack faces is very small, the faces will be attached under compressive loading. This attachment is reproduced by introducing a solid modeling and contact condition on the crack faces. The results revealed that, if the gap is small, the presence of the crack and the crack surface contact are strongly affected by the buckling and collapse behaviors.

In the present study, an experimental apparatus is developed for examining the buckling and collapse behaviors of a cracked panel subjected a sequential tensile and compressive loading. Two cracked steel panel specimens with different crack lengths and one intact panel specimen are employed. The load-displacement curves and CODs are measured. The mechanical behaviors of the cracked panel are examined via the FE computation. It is noted that the test specimen is very thin and there is a small gap, no crack face contact occurs. Cracked panel experiments have been performed in various studies *i.e.*, [41-45]. However, studies considering a cracked steel panel subjected to sequential tensile and compressive loading are rare.

The present paper is organized as follows. The experimental study is pre-

sented in Section 2. FE computation is carried out to examine the buckling and collapse behaviors in Section 3. Results and discussion are presented in Section 4. The concluding remarks are drawn in Section 5.

## 2. Experimental study

### 2.1. Experimental apparatus

An experimental apparatus was developed for examining the buckling behavior of an intact panel under monotonic compressive loading in our laboratory [47]. The present work, the design is modified and a new apparatus is developed for investigating the buckling and collapse behaviors of a cracked thin panel subjected to sequential tensile and compressive loads.

The parts (see Fig. 1(a)) are fabricated from a structural steel and are composed of a shaft, jigs and spacers. A test specimen and spacers are shown in Fig. 1(b). The spacer thickness and the material are the same as those of the specimen. The specimen is supported by the jigs and bolts that suppress the out-of-plane deformation as illustrated in Fig. 1(c). To allow clamping of the specimens, serrations are introduced to the surface of Jig1, Jig3, Jig5 and lower part of Jig6, as presented in Fig. 1(a) and (c). Both edges of the specimen can move smoothly by inserting the spacers between Jig2 and Jig6 as well as between Jig4 and Jig6. The assembled illustration is drawn in Fig. 1(d). Here, we define the front side and back side of the apparatus.

The setting for the experiments is presented in Fig. 2(a)-(c). A universal testing machine (Shimadzu Autograph) is employed. As shown in Fig. 2(a), top and bottom of the apparatus are connected to the machine. A specimen is positioned, as presented in Fig. 2(b). The specimen is fixed with bolts as shown Fig. 2(c). All edges of the specimen are supported by the jigs to suppress the out-of-plane deformation. Grease is placed between the jigs and both edges of the specimen to ensure the smooth movement. Under displacement control, Jig1 and Jig5 (see Fig. 1(c)) can move with the specimen through the shaft.

### 2.2. Test specimens

A schematic of a test specimen is illustrated in Fig. 3(a). The longitudinal length is  $2L(=390\text{ mm})$  and the width is 200 mm. The panel thickness is 0.8 mm. The load is applied along the longitudinal direction. A through crack  $2a$  is located at the center of the panel ( $L$  from bottom of the specimen) and perpendicular to the loading direction. The specimen is clamped by the

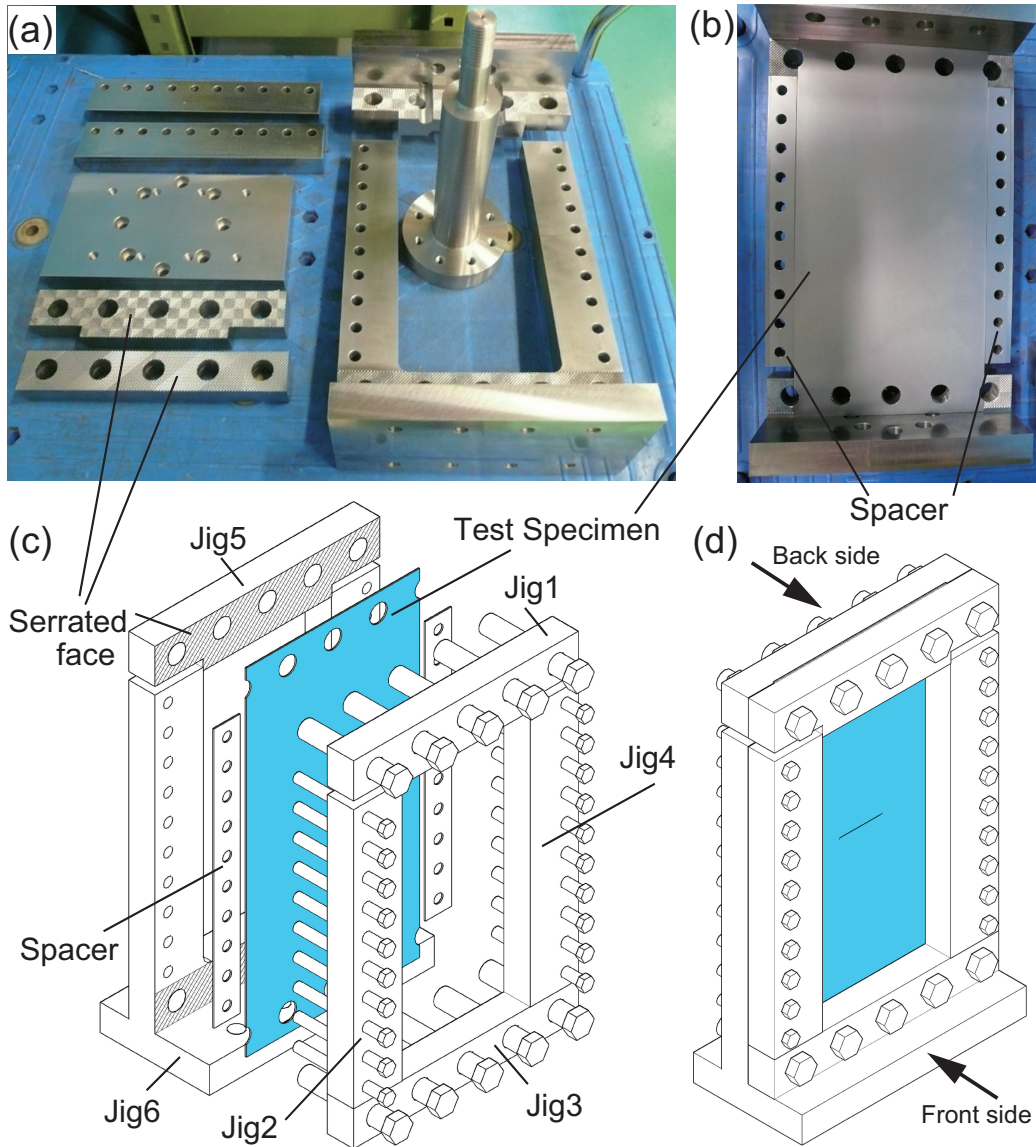


Figure 1: A newly developed experimental apparatus. [(a) Steel parts, (b) A test specimen and spacers, (c) Parts assembly with specimen, spacer and jigs, (d) Assembled].

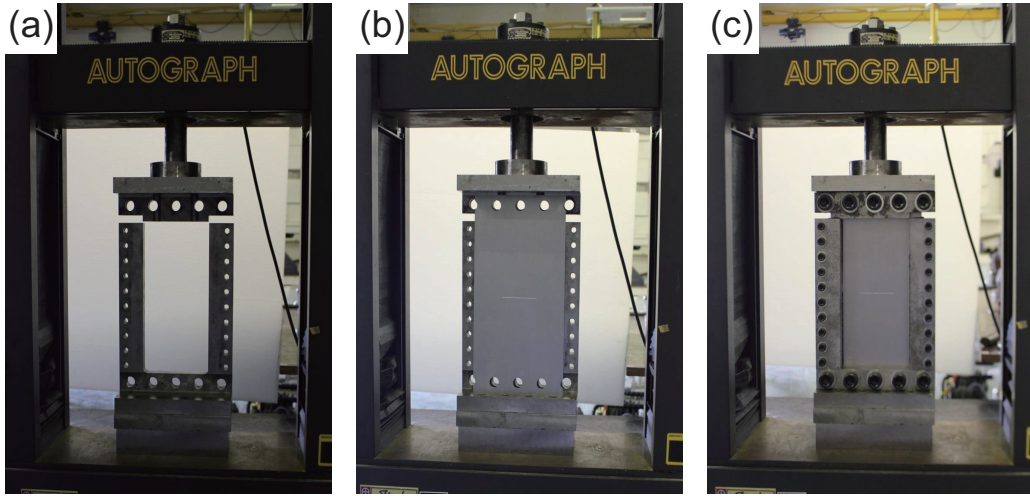


Figure 2: Setting for the experiments. [(a) Before the specimen installation, (b) With specimen, (c) Assembled].

jigs. The non-shaded region  $160 \times 310$  mm is a target domain of the testing as shown in Fig. 3(b). The aspect ratio is approximately two. A three half waves buckling mode can be obtained theoretically for an intact panel with all edges clamped [1]. To evaluate crack opening/closing displacements, measurement points (plus marks) are placed 20 mm above/below the crack (details of the crack geometry are presented in Fig. 3(c)). The crack is obtained using an electrical discharge machining technique (wire size is 0.2 mm). A picture of the  $2a=50$  mm crack is taken in Fig. 3(d). The width of the gap is  $\sim 0.25$  mm.

Three types of specimens are considered, namely an intact specimen and cracked specimens with different crack lengths. An intact specimen is shown in Fig. 4(a). Cracked specimens with  $2a=50$  mm and 75 mm are presented in Fig. 4(b) and (c), respectively. Tensile and compressive loads are applied to the specimens. The specimen is composed of a Steel Plate Cold Commercial (SPCC) material. The chemical compositions of the material are presented in Table 1.

The material parameters are determined prior to the buckling testing. Specimens for the tensile test are taken from the same steel panel. Three specimens (TS1-TS3) are employed and the material parameters are determined using strain gauges. The load-displacement curves obtained exhibit the same tendency as shown in Fig. 5. From the strain gauge data, a Young's

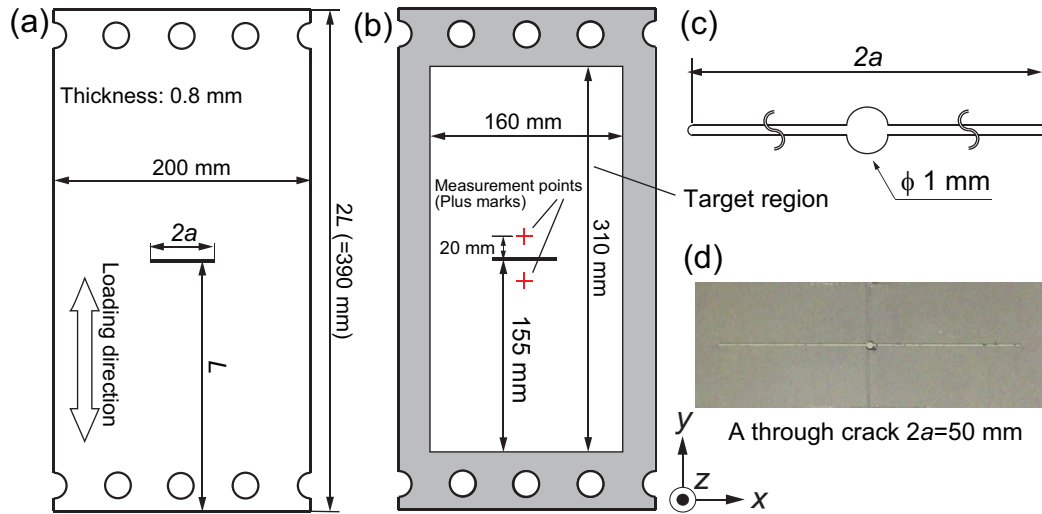


Figure 3: Test specimen for the experiment. [(a) Size and dimension of the cracked specimen, (b) Target region for the testing, (c) Crack geometry, (d) Close-up view of a crack for  $2a=50 \text{ mm}$ ].

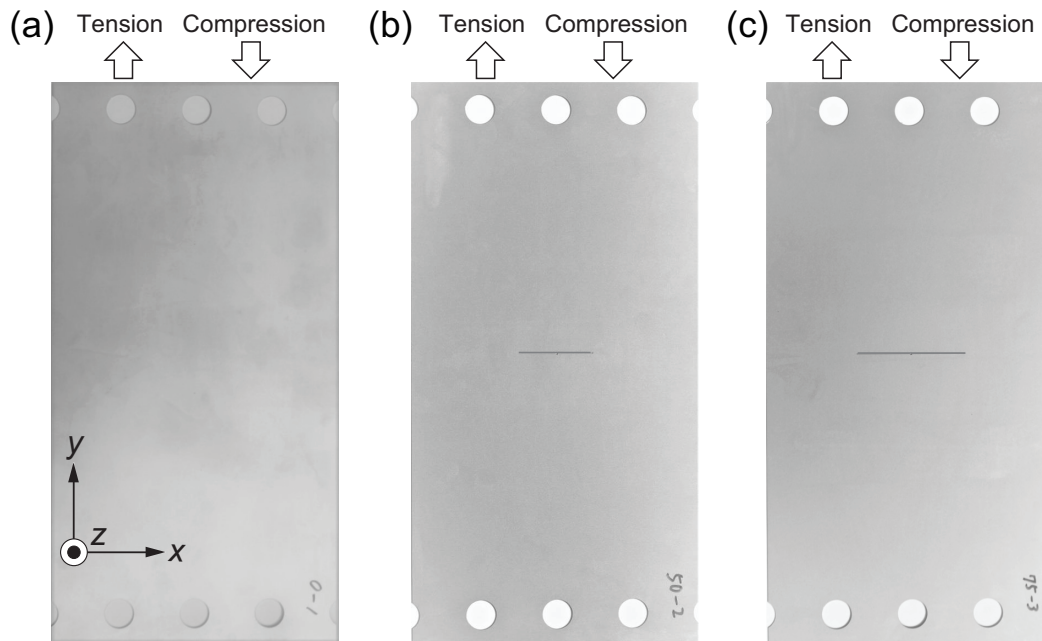


Figure 4: Overall view of test specimens with different crack length. [(a)  $2a=0 \text{ mm}$ , (b)  $2a=50 \text{ mm}$ , (c)  $2a=75 \text{ mm}$ ].

Table 1: Chemical composition of the steel material (SPCC).

%C	%Mn	%P	%S
0.04	0.18	0.14	0.06

modulus  $E$  is 215.9 GPa and Poisson’s ratio  $\nu$  is 0.34 are obtained. A bi-linear isotropic hardening model illustrated in Fig. 6 is utilized as it is an approximation to the stress-strain curve of the material. The yield stress  $\sigma_Y$  and hardening ratio  $E_{tan}$  are 270 MPa and 2,256 MPa, respectively.

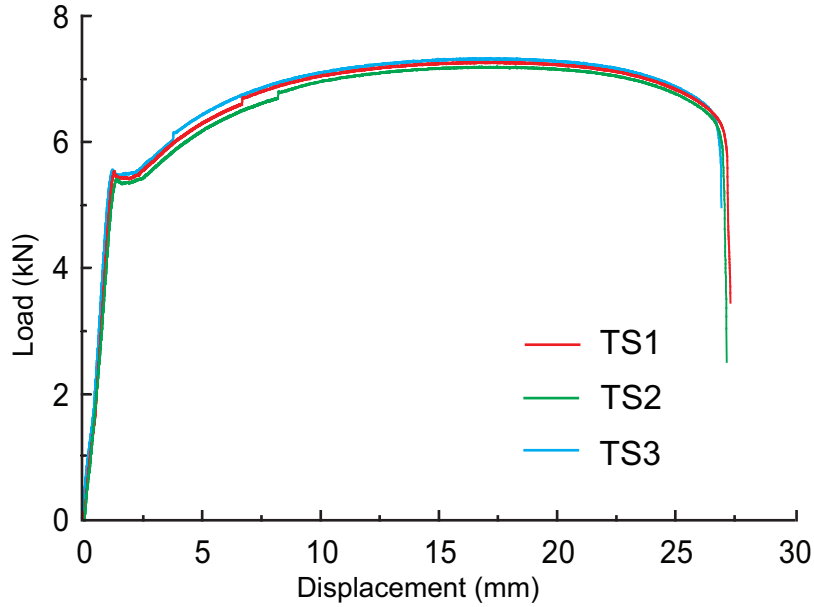


Figure 5: Load-displacement curves of the tensile test (TS1-TS3).

### 2.3. Experimental results

Tensile (T) and compressive (P) loads are sequentially applied to the intact and cracked test specimens. After the preliminary test, a total of eight specimens are tested under a displacement control. A load-displacement history applied to the specimens is shown in Fig. 7. A monotonic tensile displacement is applied first and continued by a compressive displacement immediately. A schematic of the typical load-displacement curve is illustrated in Fig. 8(a). In the figure, the amplitude of the forced displacement

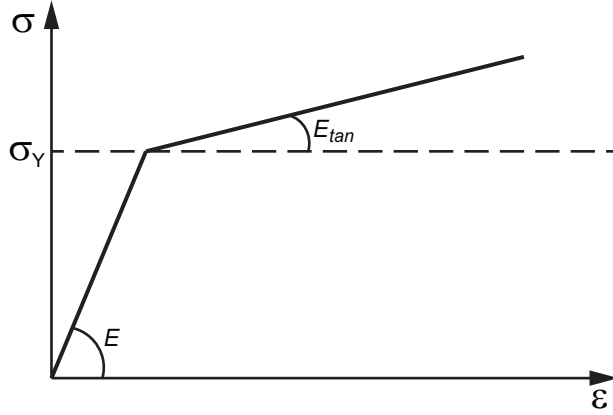


Figure 6: A bilinear isotropic hardening model.

and load against the displacement are plotted on the horizontal axis and vertical axis, respectively. During the testing, the panel experiences tensile load under the tensile displacement. The specimens undergo major plastic deformation, which is manifested in the region near point A. Compressive displacement is applied after the maximum load is reached under the maximum displacement (which occurs at point B). The compressive load leads to buckling of the panel. The ultimate strength of the specimen occurs at point C, and the load decreases gradually at point D. The load-displacement curves of the intact and cracked specimens with  $2a=50$  mm and 75 mm cracks are shown in Fig. 8(b)-(d), respectively.

Two intact specimens (TCS1, TCS2) are employed, and are subjected to forced tensile displacements of 3.0 mm and 2.5 mm, respectively, as shown in Fig. 8(b). The loads increase monotonically under the tensile displacement, and almost the same initial stiffness is observed. A major plastic deformation occurs at  $\sim 1.7$  mm corresponding to point A of both specimens. Under the subsequent tensile displacement, further deformation of the panel occurs until the maximum displacement is reached at point B. The specimens exhibit almost the same stiffness during the compressive displacement and, in each case, the ultimate strength occurs at point C. The loads decreased after the peak load at point D. Although the forced displacement amplitude is different, good correlation between the curves of the two intact specimens is observed.

Three specimens with a 50 mm crack (TCS3-TCS5) were tested. The load-displacement curves are shown in Fig. 8(c). A 2.5 mm forced displace-

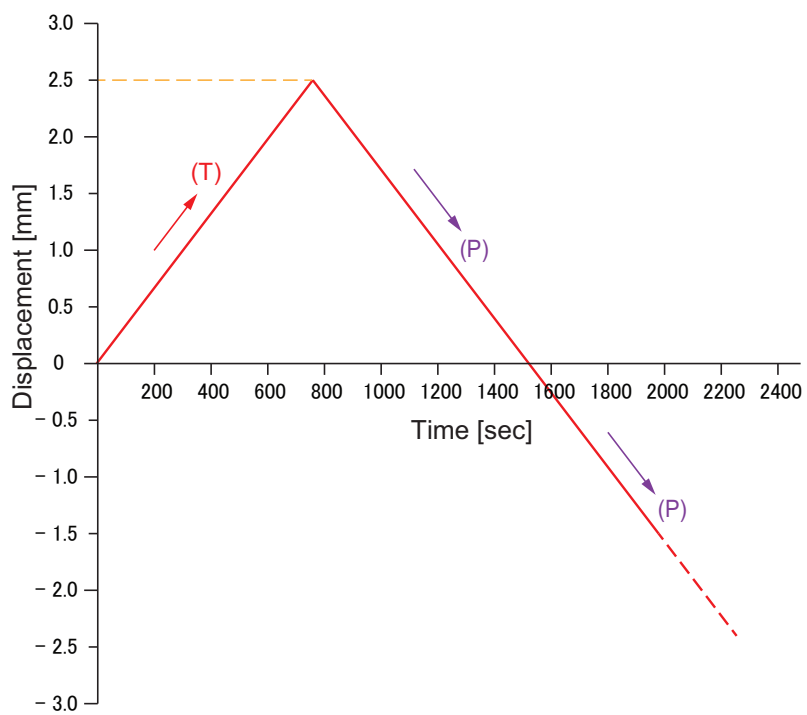


Figure 7: The load-displacement history applied for the test specimens.

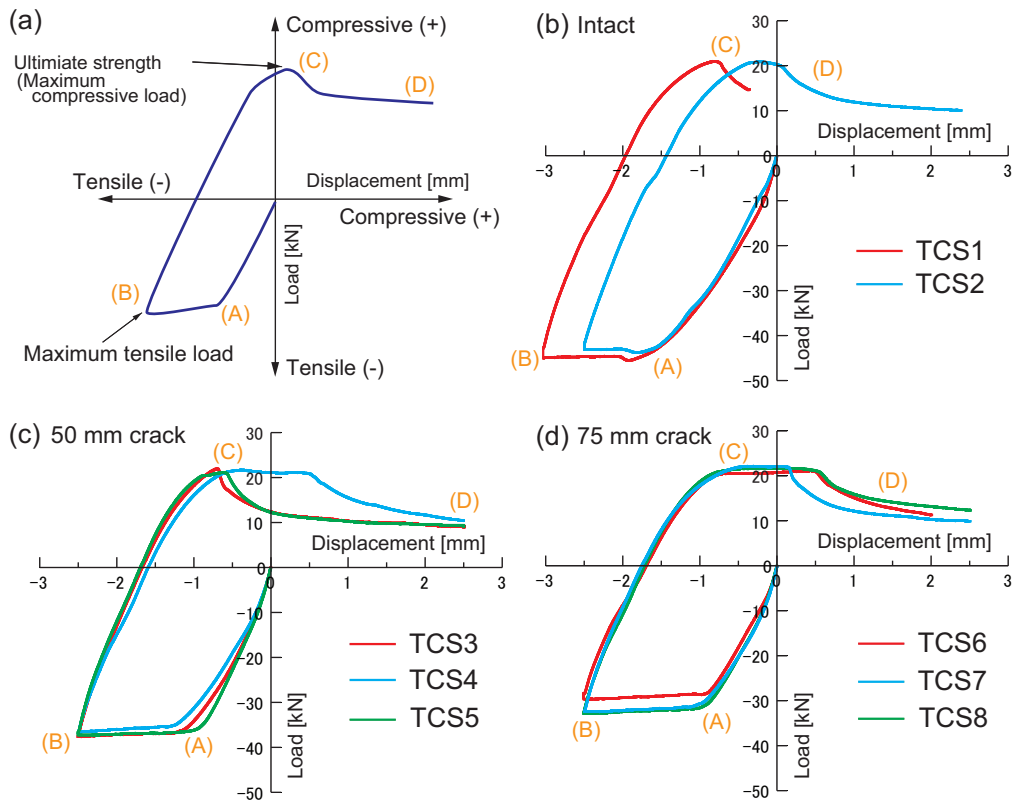


Figure 8: Load-displacement curves for the test specimens. [(a) A typical load-displacement curve of a sequential tensile and compressive loading, (b) Intact specimens (TCS1, TCS2), (c) 50 mm cracked specimens (TCS3-TCS5), (d) 75 mm cracked specimens (TCS6-TCS8)].

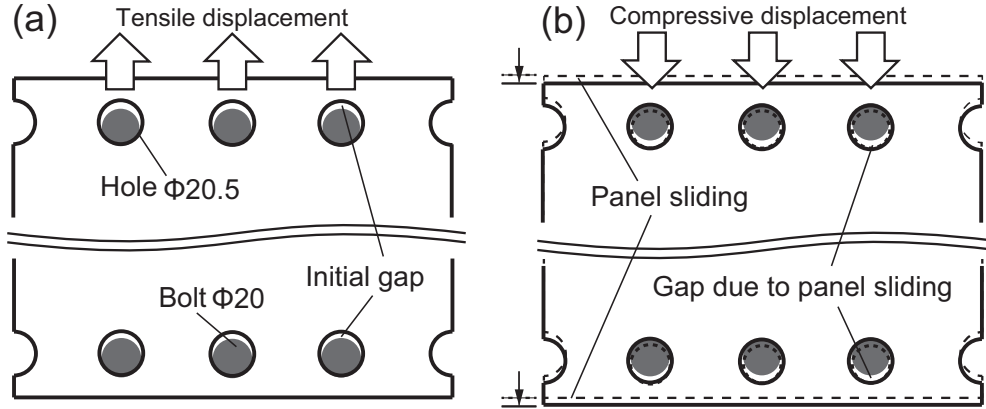


Figure 9: A panel sliding and contact with bolts. [(a) Tensile loading case (Initial setting), (b) Compressive loading case (Panel sliding)].

ment is applied to each specimen. The initial stiffness of the specimens differs slightly under the tensile displacement, but the same trend is observed after the major plastic deformation at point A. The loads increase slightly and reach the peak at point B under the maximum displacement. Moreover the peak loads are the same. After the compressive displacement is applied, the specimens exhibit the same stiffness and the ultimate strength of each specimen occurs at point C. The peak loads are almost the same. Afterward, the load decreases under the subsequent compressive displacement toward point D. The curves exhibit the same tendency in three specimens until the curves attain the ultimate strength.

Additionally, the load-displacement curves of cracked specimens with 75 mm crack are shown in Fig. 8(d). Three specimens (TCS6-TCS8) are employed. The same initial stiffness is observed. For the intact and 50 mm cracked specimens, a significant plastic deformation occurs at point A. The loads increase slightly until point B. Subsequently, the load decreases under the compressive displacement, and the curve reaches ultimate strength at point C. In addition, the loads decreased at point D. The curves of the 50 mm cracked specimens exhibit the same trends up to the point where the ultimate strength of the 75 mm cracked specimens is reached.

Although the experimental results reveal good correlation between the load-displacement curves of the intact and cracked test specimens, in some cases, the curves differ modestly in the regions near point C, *i.e.*, where the ultimate strength is reached. When the curves reach point C (Fig. 8(b)-(d)),

the load decreases gradually for TCS1-TCS3 and TCS5. However, in the curves corresponding to TCS4 and TCS6-TCS8, the value remains close to the ultimate strength prior to the load reduction. This results from sliding between the specimen and jigs and contact between the specimen and bolts.

A schematic of the contact phenomenon between the specimen and bolts is drawn in Fig. 9(a) and (b). The position of the specimen and bolts is shown in Fig. 9(a). The hole diameter and the bolt diameter are 20.5 mm and 20.0 mm, respectively. The surface of the jigs is serrated to firmly clamp the specimen, as presented in Fig. 1(a) and (c). However, a panel sliding sometimes occurs due to the gap between the holes and bolts as shown in Fig. 9(b). This may have contributed to the differences in the regions around the point of their ultimate strength in the load-displacement curves. Although a local yielding (*e.g.*, between the bolts and holes) may generated, no major sliding occurs under the tensile displacement because the bolts and the panels are attached as the initial setting.

The load-displacement curves including tensile and compressive peak loads are investigated. For example, as shown in Fig. 8(b)-(d), the peak load of the intact panels  $\sim 45$  kN, while the peak loads of the 50 mm and 75 mm cracked specimens are  $\sim 35$  kN and 30 kN, respectively. The peak load may have decreased due to the presence of the crack. The load reduction increases with increasing crack size. However, almost the same ultimate strength value ( $\sim 20$  kN) is obtained in all cases. The ultimate strength behaviors are examined in the numerical simulation.

The buckling and collapse behaviors for intact and cracked specimens with 50 mm and 75 mm crack are shown in Fig. 10(a)-(c), respectively. The behaviors correspond to the post-ultimate strength state, *i.e.*, point D in Fig. 8(b)-(d). The photos are taken from the front side and the back side, as shown in Fig. 1(d). Fig. 10(a) is the final buckling shape after point D of an intact specimen for a preliminary test. The buckling mode is characterized by three half waves that corresponds with a theoretical elastic buckling mode of a panel with all clamped edges. Three half waves are also observed for the 50 mm cracked specimens (TCS4), where the deformation is localized around the crack. These waves and localization also occur for the 75 mm cracked specimen (TCS7).

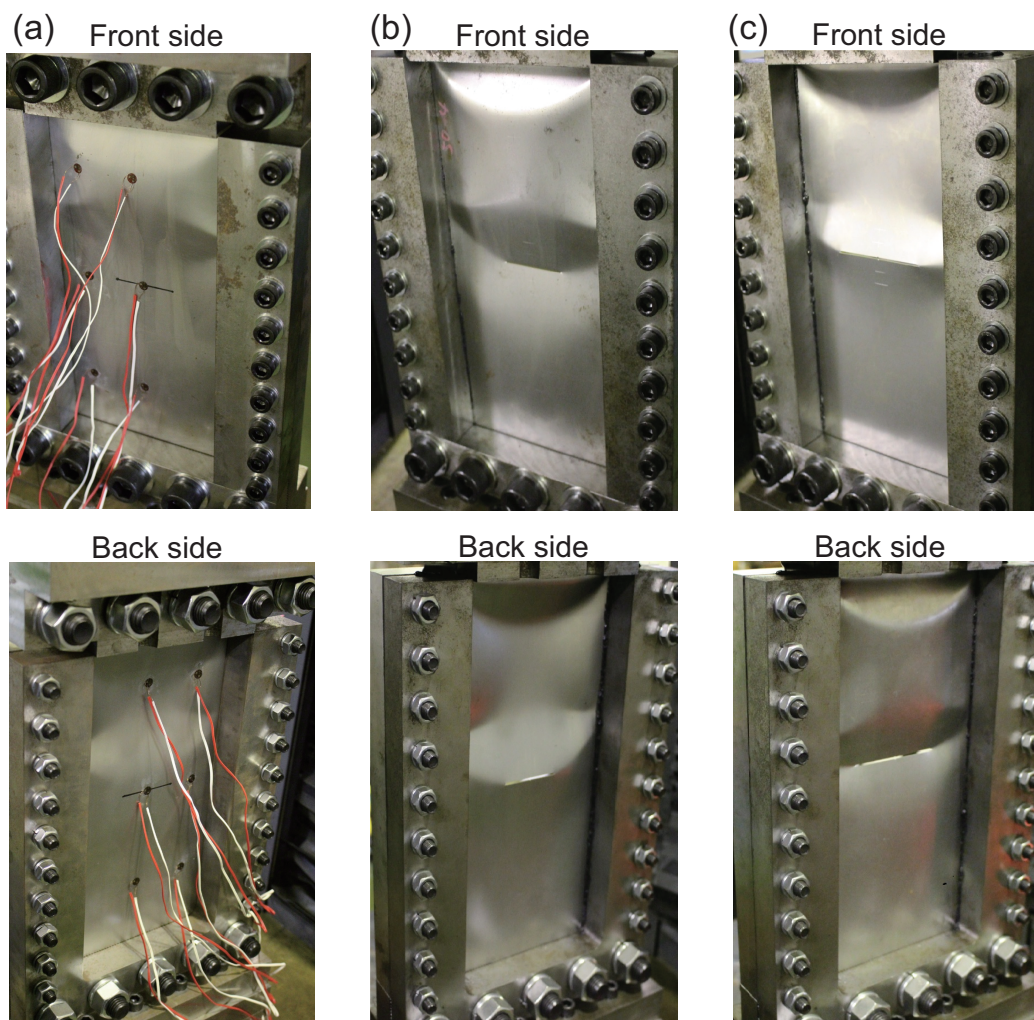


Figure 10: Collapse behaviors of the test specimens. [(a) Intact specimen (A preliminary test specimen), (b) 50mm cracked specimen (TCS4), (c) 75mm cracked specimen (TCS7)].

### 3. FE modeling

The buckling and collapse behaviors of the test specimens subjected to a sequence of tensile to compressive loading are evaluated by means of a numerical investigation. A schematic illustration of the experimental apparatus and test specimen is shown in Fig. 11(a). Modeling of the displacement BCs is illustrated in Fig. 11(b). As the basic concept, upper and lower parts of the specimen are clamped with jigs. Forced tensile and compressive displacements are applied to the upper part of the specimen. Both sides of the specimen can move smoothly but out-of-plane deformation is suppressed. For the sake of simplicity, holes and bolts are neglected.

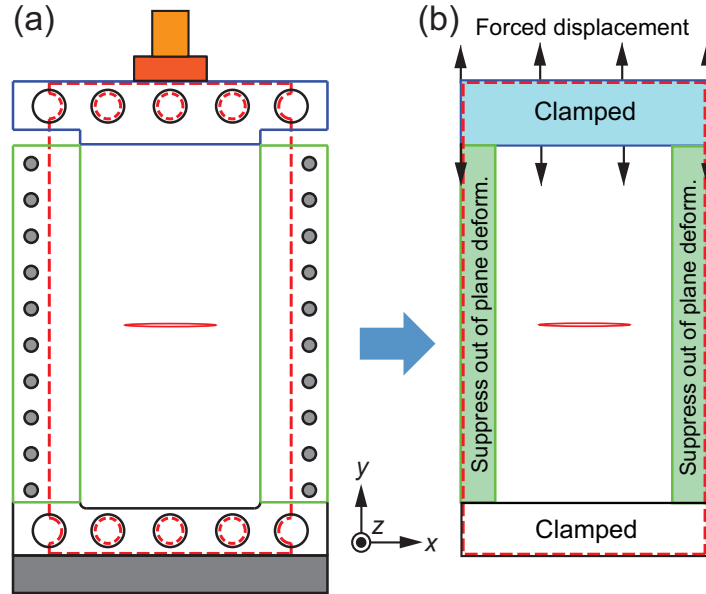


Figure 11: Numerical modeling of the experimental apparatus and test specimen. [(a) A schematic illustration of the apparatus and specimen, (b) Numerical modeling].

The FE model is shown in Fig. 12(a). Commercial FE software LS-DYNA [48] is employed. Fully Integrated Shell Element (ELFORM=16) is used for the shell FE modeling. The specimen is divided into 40 elements in the  $x$ -direction and 78 elements in the  $y$ -direction. A through crack is modeled using duplicated nodes. The contact condition between the crack faces is neglected. The gap of the crack 0.25 mm is created as illustrated in the Fig. 12(b). Furthermore, 10 and 15 elements are employed for the

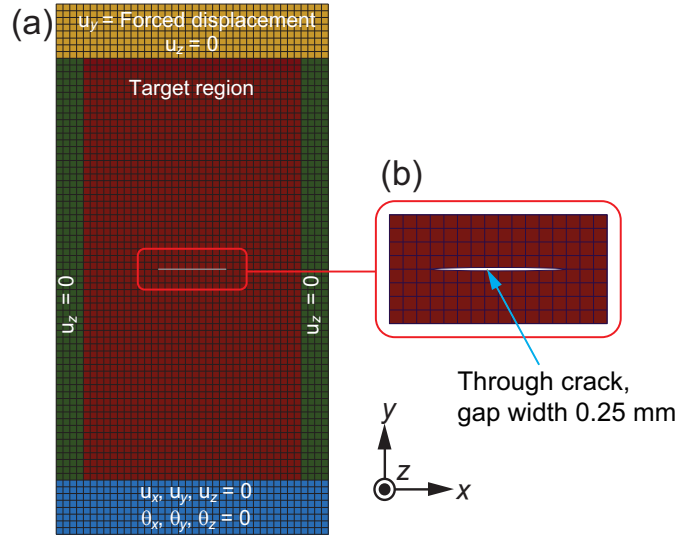


Figure 12: FE modeling of the cracked specimen. [(a) Shell FE model, (b) FE modeling of a through crack].

modeling of 50 and 75 mm cracks, respectively. A static implicit method is employed.

The displacement BCs are presented in Fig. 12(a). The FE model is divided into four parts. All DOFs are fixed in the blue colored part to reproduce the clamp condition of jigs. The  $z$ -direction is imposed in the green colored part to suppress the out of plane deformation of the specimen. Moreover, forced tensile and compressive displacements are applied in the yellow colored part, and the out-of-plane deformation is suppressed. All DOFs are free for the red colored part and a half wave initial deflection. The initial deflection with 10% amplitude of the panel thickness, *i.e.*, 0.08 mm is imposed in the intact and cracked panel models. In addition, the material parameters obtained from the tensile testing are used.

The experimental results are elucidated by considering three loading conditions (the schematics are presented in Fig. 13(a)-(c)). Because the numerical simulation is simplified the experiment behaviors, *e.g.*, sliding of the specimens, different load amplitude is employed. In the first case, a monotonic compressive displacement is considered (see Fig.13(a)). In the second case, a tensile displacement is enforced until  $\varepsilon_y/\varepsilon_Y = -1.0$  and a compressive displacement is then applied, as shown in Fig. 13(b). The  $\varepsilon_y$  and  $\varepsilon_Y$  correspond to the average strain calculated from the forced displacement along the loading

direction and yield strain of the specimen, *i.e.*,  $\varepsilon_Y = \sigma_Y / E$ , respectively. In the third case, a tensile displacement is applied until  $\varepsilon_y / \varepsilon_Y = -2.0$  and a compressive displacement is subsequently applied. The first, second and third cases are referred to as loading cases (P), (T)-(P), 100% and (T)-(P), 200%, respectively. Similar to the load-displacement history in the experiments, uniaxial load-displacement is also applied to the intact and cracked panel models. The load-displacement histories are shown in Fig. 14 for loading cases (P) to loading case (T)-(P), 200% corresponds to Fig. 13(a) to Fig. 13(c), respectively.

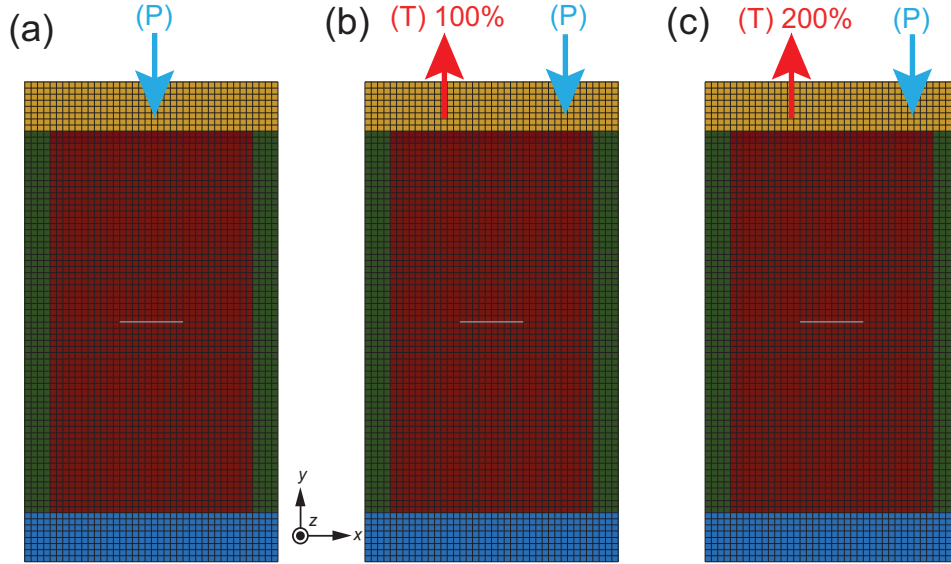


Figure 13: Loading conditions for the intact and cracked panel models. [(a) Loading case (P), (b) Loading case (T)-(P), 100%, (c) Loading case (T)-(P), 200%].

## 4. Results and discussion

### 4.1. Loading case (P)

A monotonic compressive displacement case, *i.e.*, loading case (P), is examined. An intact model and crack models with 50 mm and 75 mm cracks are employed (the results are shown in Fig. 15). The normalized stress  $\sigma_y / \sigma_Y$  and normalized strain  $\varepsilon_y / \varepsilon_Y$  are plotted on the vertical axis and horizontal axis, respectively.  $\varepsilon_y$  is analyzed by the forced displacement  $u_y$  in Fig. 12 by dividing the panel length, *i.e.*, 310 mm.  $\sigma_y$  is evaluated by reaction

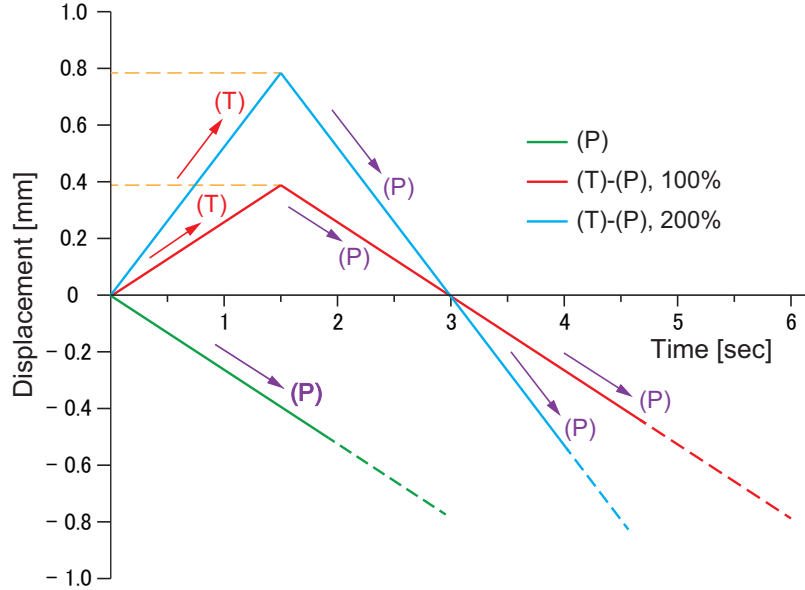


Figure 14: Load-displacement histories applied to the intact and cracked panel models for the loading cases (P), (T)-(P), 100%, and (T)-(P), 200%.

force of the forced displacement. The cross section area of the intact panel is employed for the normalization. The deflection of the intact and crack models is investigated, as shown in Fig. 16(a)-(c). Fig. 16(a) shows the results of the intact model. The results of the 50 mm and 75 mm crack models are shown in Fig. 16(b) and (c). For clear visualization, the deformation is magnified five times.

As shown in Fig. 15, a panel buckling occurs around point A. The initial stiffness among the three models are slightly different. The intact panel case is greater than the cracked panel cases. Because strain localization occurs around the crack tip, the initial stiffness of the cracked models is reduced. However, the localization is only occurred at the crack tip, therefore no big difference can be seen in the initial stiffness. If the same path is taken after point A, the ultimate strength in each model occurs at point B. For the intact model, three half waves are observed (Fig. 16(a)), consistent with the results of the experiment. Three half waves are also observed for the 50 mm crack model, as shown in Fig. 16(b). The amplitude of the 75 mm crack model (Fig. 16(c)) is lower than that of the 50 mm crack model. Furthermore, the buckling deformation is suppressed due to the presence of the crack, because

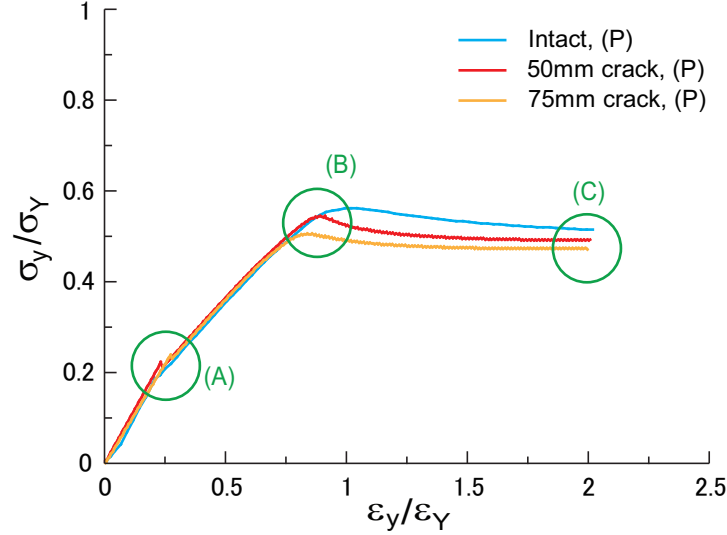


Figure 15: Normalized stress-strain curves for loading case (P) for intact and cracked models.

transfer of the axial load through the crack faces is prevented. The load decreases toward point C under the subsequent compressive displacement. The ultimate strength of the crack models is lower than that of the intact model due to presence of the crack. Moreover, the ultimate strength of the 50 mm crack model is higher than that of the 75 mm crack model.

The stress distributions associated with the ultimate strength at point B (see Fig. 15) of the intact model and crack models considering 50 mm and 75 mm cracks are shown in Fig. 17(a)-(c), respectively. The Mises stress of the panel top surface is illustrated. Yielding occurs in the red colored region. The trends observed for the yielding region are similar for cases with/without a crack and are independent of the crack length. Therefore, in the present case, the ultimate strength decreases only modestly even in the case of a relatively large transverse crack (50% of the panel width).

#### 4.2. Loading case (T)-(P), 100%

A sequential tensile and compressive loading, *i.e.*, (T)-(P), 100%, is examined. The normalized stress-strain curves for the intact models and crack models with 50 mm and 75 mm cracks are shown in Fig. 18. For applied tensile displacement of up to  $\varepsilon_y/\varepsilon_Y = -1.0$ , yielding occurs slightly at point A in the intact model. The unloading path after the peak tensile load is almost

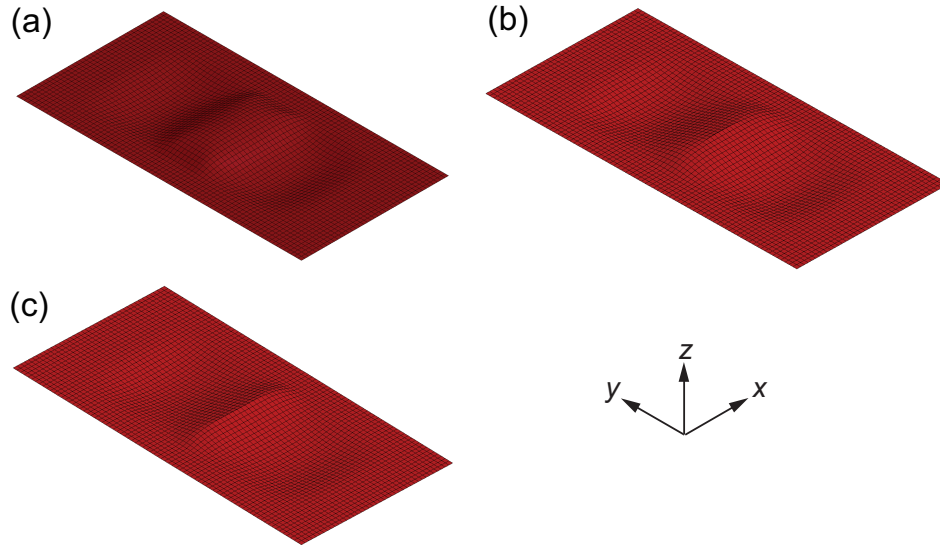


Figure 16: Deflection at the ultimate strength for loading case (P) (The deflection is magnified five times for the visualization). [(a) Intact model, (b) 50 mm crack model, (c) 75 mm crack model].

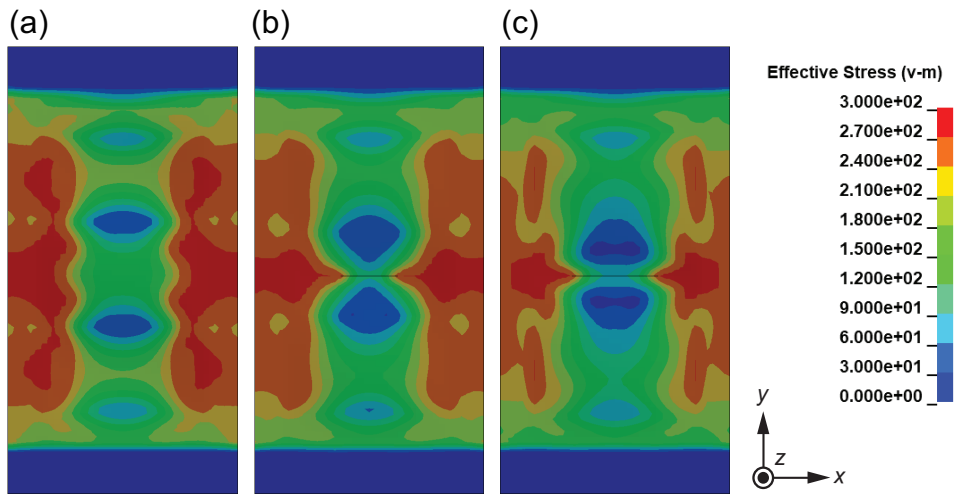


Figure 17: Mises stress distribution at the ultimate strength for loading case (P). [(a) Intact model, (b) 50 mm crack model, (c) 75 mm crack model].

identical to that of the tensile displacement case. The ultimate strength of the panel occurs at point B, and the load decreases toward point C. The curve obtained for the model is almost same as that of the intact model considering samples under a monotonic compressive load (see Fig. 15).

In the 50 mm and 75 mm crack models, yielding occurs at the maximum tensile displacement, *i.e.*, at points D and F, respectively. The contour diagram of the Mises stress distribution occurring at the maximum tension in the intact and crack models is shown in Fig. 19. For the intact model, yielding occurs along the entire panel, whereas in the crack models yielding is localized due to the presence of the crack. When a compressive displacement is applied, the ultimate strength of the panels occurs at points E and G (the strength of the cracked panels is slightly lower than that of the intact case). The ultimate strength occurring in the 75 mm crack model is lower than that of the other models.

The buckling and collapse behavior of the cracked models is further investigated by determining the equivalent plastic strain distribution of the 50 mm crack model. The distributions occurring at the maximum tension, ultimate strength and post ultimate strength are shown in Fig. 20(a)-(c), respectively. The deflection is also presented (see Fig. 21(a)-(c)). In the maximum tensile loading case (Fig. 20(a)), the plastic strain extends from the crack tip to the panel edge. At the ultimate strength in Fig. 20(b), a new plastic region is generated parallel to the crack due to localization of the deformation (see Fig. 21(b)). The panel is further deformed under the subsequent compressive displacement in Fig. 21(c) and the plastic strain region expanded around the crack tip as presented in Fig. 20(c).

#### 4.3. Loading case (T)-(P), 200%

Loading case (T)-(P), 200% is examined. The corresponding normalized stress-strain curves are presented in Fig. 22. For the intact model, yielding occurs at point A and the displacement increases until point B is reached. After the compressive displacement is applied, the ultimate strength occurs at point C. The load decreases toward point D. Similar trends are observed in the curves for the crack models. The maximum tensile loads decrease, as shown for points E and F of the 50 mm and 75 mm crack models. After the compressive displacement is applied, the ultimate strength associated with each model occurs at points G and H, respectively.

The deflection at the post ultimate strength of the intact and crack models with 50 mm and 75 mm crack are shown in Fig. 23(a)-(c). This deflection

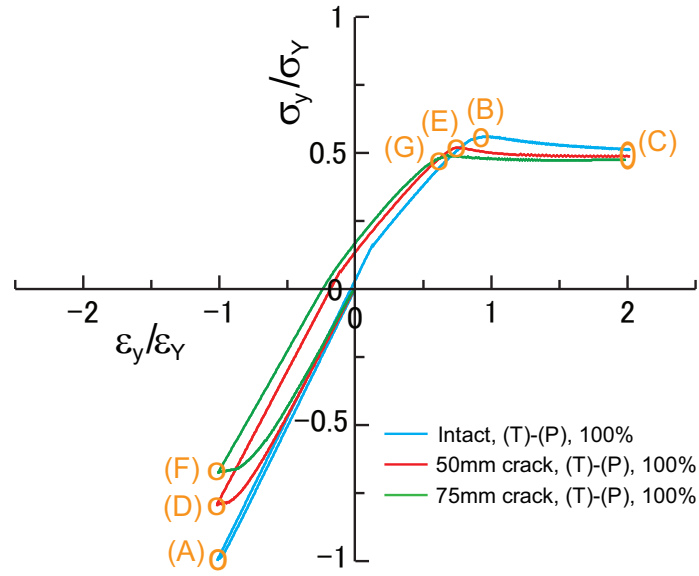


Figure 18: Normalized stress-strain curves for loading case (T)-(P), 100% of the intact and crack models.

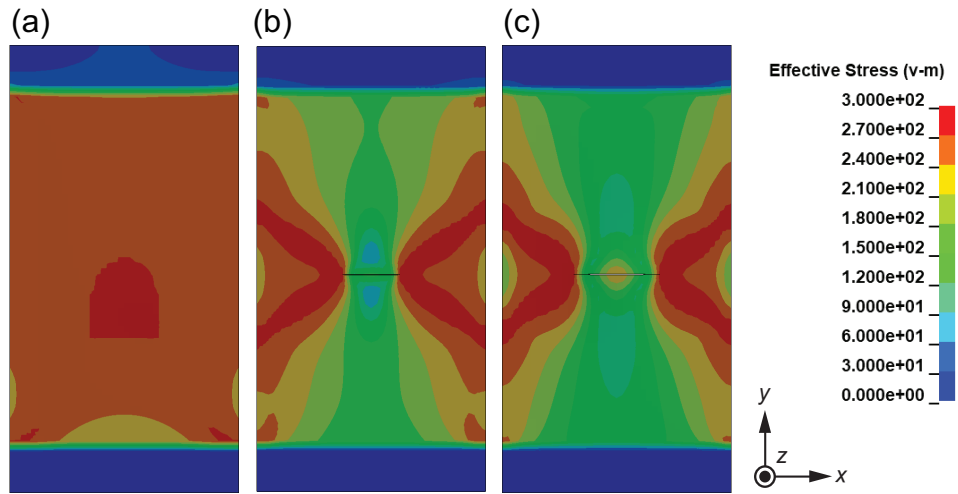


Figure 19: Mises stress distribution at the maximum tension for loading cases (T)-(P), 100%. [(a) Intact model, (b) 50 mm crack model, (c) 75 mm crack model].

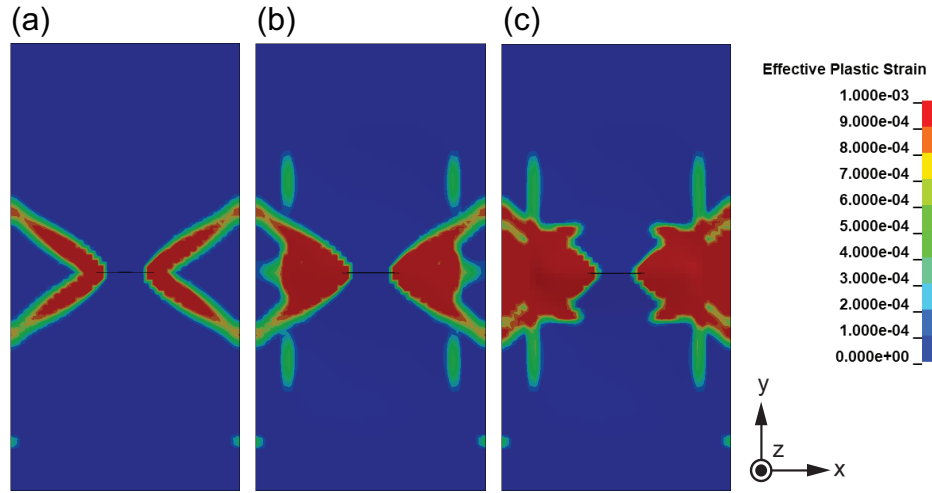


Figure 20: Equivalent plastic strain distribution of 50 mm crack model for loading case (T)-(P), 100%. [(a) maximum tension, (b) ultimate strength, (c) post ultimate strength].

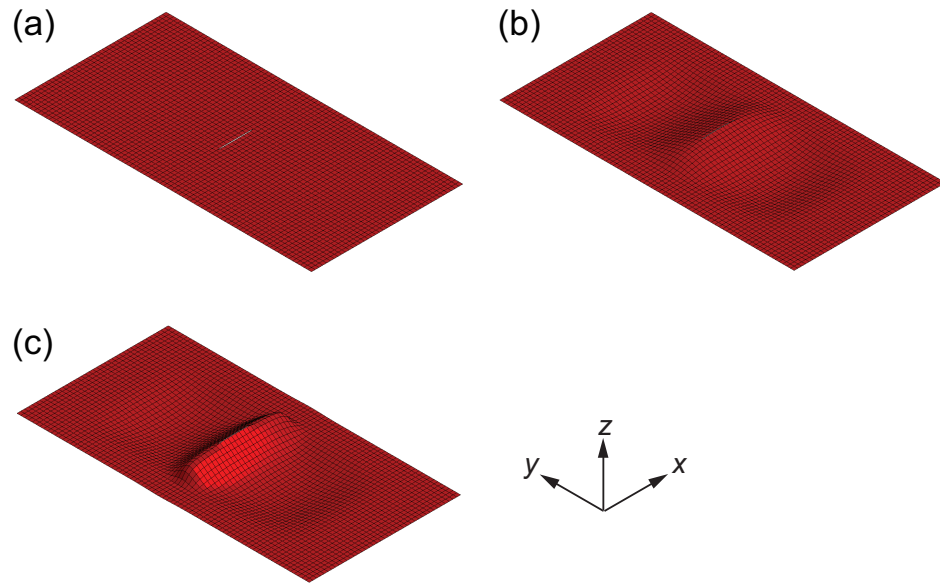


Figure 21: Deflection for the 50 mm crack model under loading case (T)-(P), 100%. [(a) maximum tension, (b) ultimate strength, (c) post ultimate strength].

corresponds to point D in Fig. 18. Three half waves are apparent but considerable localization of deformation is observed.

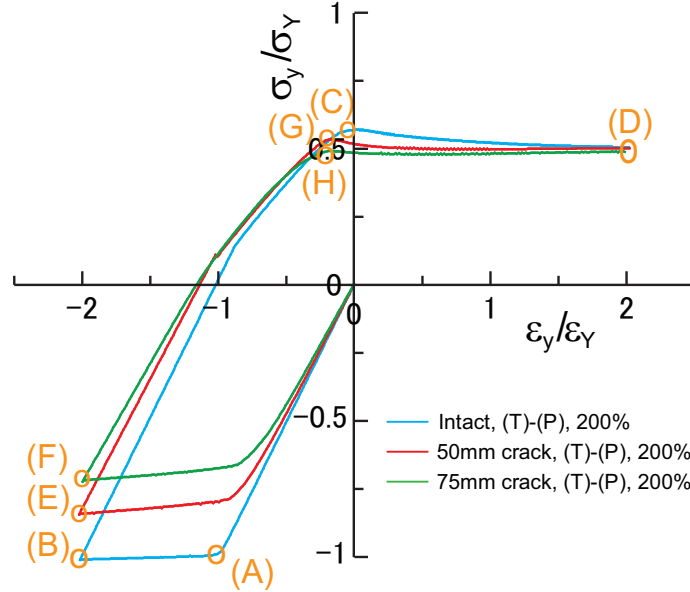


Figure 22: Normalized stress-strain curves for loading case (T)-(P), 200% for intact and crack models.

#### 4.4. Comparison with experimental results

The load-displacement curves of TCS2, TCS5 and TCS8 are shown in Fig. 24(a). Additionally, the curves corresponding to loading case (T)-(P), 200% is presented in Fig. 24(b). The experimentally determined and simulated peak tensile load of the intact and crack cases are almost same. When a crack is included in the panel, the peak tensile load decreases, and the magnitude of this reduction increases with increasing crack size. The ultimate strength, determined from numerical methods corresponds closely to the value determined from experimental measurements. In all the cases, very similar results are obtained for the intact and cracked panels, as discussed in Section 4.1. This confirms that the experimental results are consistent and the peak tensile as well as compressive loads are well-simulated by means of the FE modeling.

The maximum tensile load and ultimate strength determined from experimental measurements correspond closely to these determined via numerical

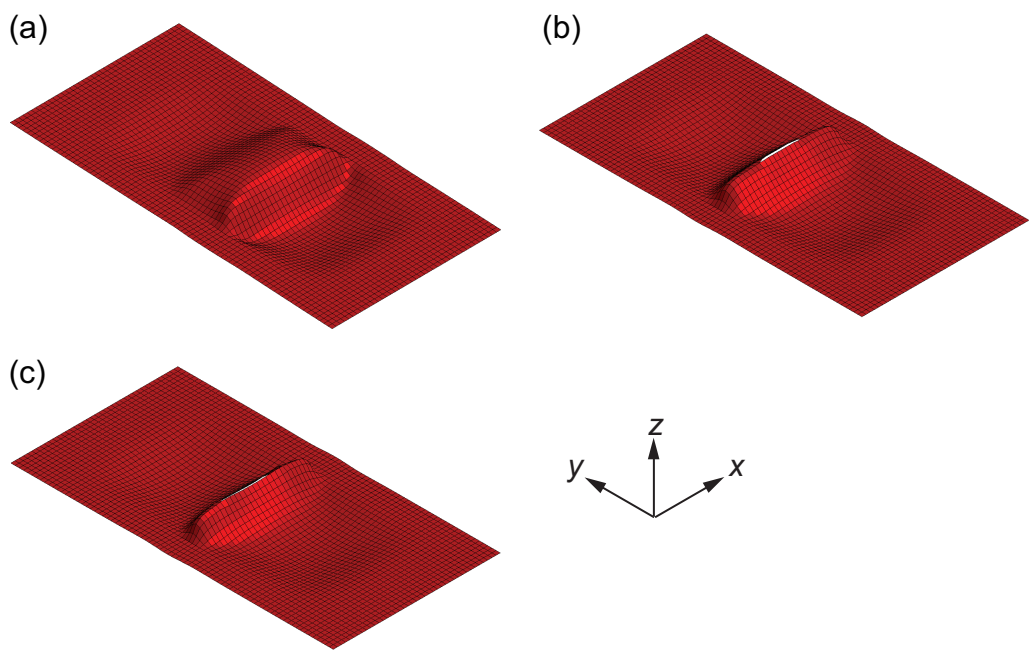


Figure 23: Deflection at the post-ultimate strength for loading case (T)-(P), 200%. [(a) Intact model, (b) 50 mm crack model, (c) 75 mm crack model].

methods, but discrepancies are observed for the displacement amplitude. As mentioned in Section 2.3, sliding and contact between the specimen and jigs occur during the experiment. However, a simplified model selected for the FE model and the displacement BCs. The sliding and contact are neglected by the model.

The buckling and collapse behavior of the cracked panel is further examined by evaluating the local deformation around the crack. A movie that shows the region around the crack is recorded during the testing, and the local distance and COD were digitized. A photo of the region around the crack is presented in Fig. 25(a). Prior to the experiment, plus marks are placed on the test specimens for measuring the local distance (distance between the crack and a cross mark: 20 mm; (see Fig. 25(b))). The distance between the cross marks is defined as the local distance and is 40 mm in the initial state. The maximum crack opening at the maximum tensile displacement is represented in Fig. 25(b). The COD is digitized.

The relation between applied stress and local deformation around crack determined from the experimental results are shown in Fig. 26(a) and (b) for specimens with 50 mm crack (TCS5) and 75 mm crack (TCS8), respectively. The local deformation associated with the local coordinate is plotted on the horizontal axis and the applied stress is plotted on the vertical axis. After the panel yields (at point A) under the tensile displacement, the tensile load increased slightly. The maximum tensile value occurs at point B. When a compressive displacement is applied, the ultimate strength occurs at point C and the load decreases at point D. Similar tendency are observed for both crack length.

The numerical results are also presented in Fig. 26(a) and (b). In the simulation, the maximum tensile displacement of the FE computation is adjusted to allow fitting of the experimentally determined maximum tensile strain at point B and the compressive displacement is applied. The simulation results and experimental results concur for cases considering 50 mm and 75 mm cracks. However, the numerical and experimental results differ to some extent after the ultimate strength (*i.e.*, point C) is reached. This results from the difference in load after the ultimate strength is reached and the measurement error due to the out-of-plane deflection of the panel as observed in Fig. 10(b) and (c).

COD is examined using the same approach. The results of COD for the 50 mm crack and 75 mm crack cases are shown in Fig. 26(a) and (b). The points A-D in Fig. 27(a) and (b) correspond to A-D in Fig. 26(a) and

(b). The COD was monotonically increased until point B and it was slightly decreased until point D. A close correspondence between the numerical and experimental results is observed, there confirming that local behavior can be simulated via FE modeling.

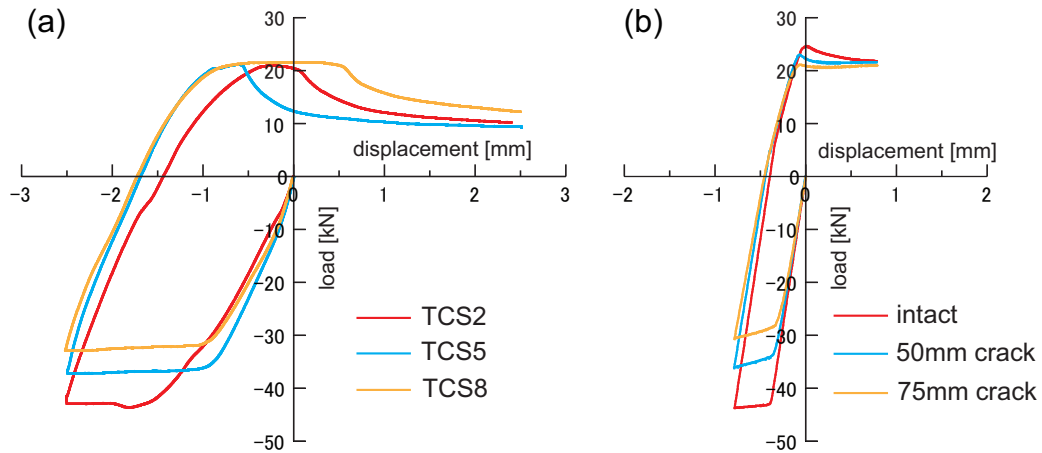


Figure 24: Comparison of the load-displacement curves obtained from experimental measurements and numerical methods. [(a) Experimental results (TCS2, TCS5, TCS8), (b) Numerical results for loading case (T)-(P), 200%].

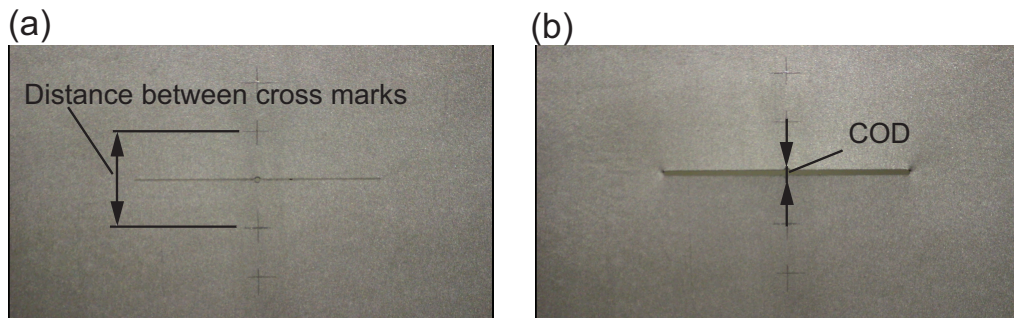


Figure 25: Definition of local distance and COD [(a) Distance between plus marks, (b) COD].

## 5. Conclusion

In the present study, the buckling and collapse behaviors of a cracked thin steel panel subjected sequential tensile and compressive loading are examined. An experimental apparatus is newly developed, and intact as well as

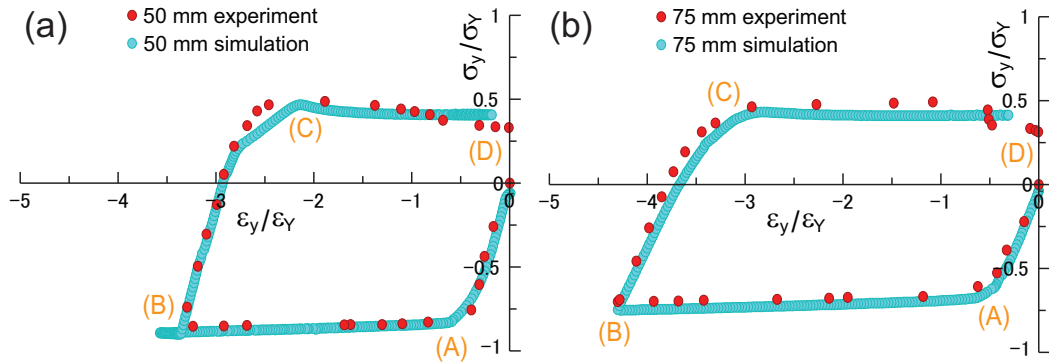


Figure 26: Comparison of stress-strain curves based on local coordinates evaluated via testing and numerical methods. [(a) 50 mm crack (TCS5), (b) 75 mm crack (TCS8)].

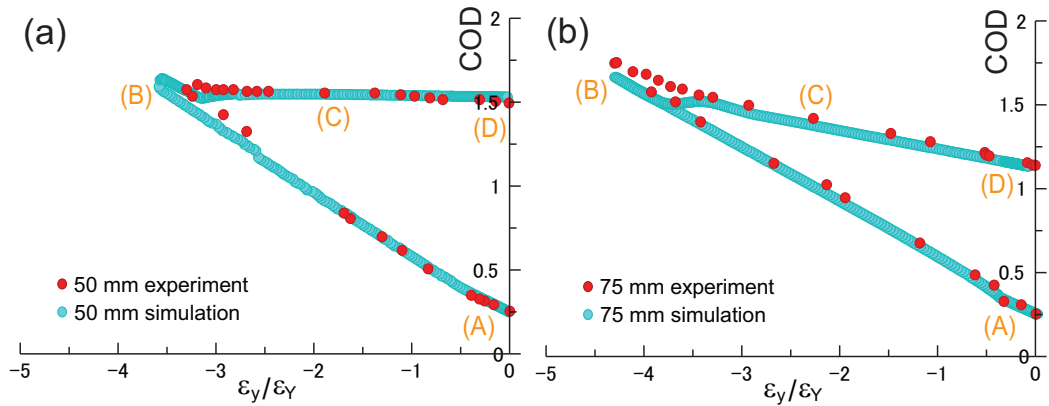


Figure 27: Comparison of COD evaluated via testing and numerical methods. [(a) 50 mm crack (TCS5), (b) 75 mm crack (TCS8).]

cracked steel panel specimens with 50 mm and 75 mm cracks are considered. The load-displacement curve and COD are obtained during the experiment. Furthermore, the buckling and collapse behaviors of the intact and cracked panels are also examined via FE computation. The results confirm that the experimental apparatus works quite well and the FE modeling is effective in simulating the mechanical behaviors. The presence of the crack and the length of the crack are strongly affected by the mechanical behaviors. In future work, low cycle fatigue crack propagation will be investigated by applying cyclic loading to the cracked panels, based on the experimental and numerical settings presented herein.

### Acknowledgements

The authors thank Tsubasa Nakajima (School of Engineering, Hiroshima University) for valuable comments on this research. This study was partially supported by the JSPS Grants-in-Aid for Scientific Research (C)(15K06632).

### References

- [1] T. Yao, M. Fujikubo, Buckling and ultimate strength of ship and ship-like floating structures, first ed. Butterworth-Heinemann, Elsevier 2016.
- [2] Z. Pei, K. Iijima, M. Fujikubo, Y. Tanaka, S. Tanaka, S. Okazawa, T. Yao. Collapse behaviour of a bulk carrier under alternate heavy loading conditions. *Int. J. Offshore Polar Eng.* 23 (2013) 232-239.
- [3] Z. Pei, K. Iijima, M. Fujikubo, S. Tanaka, S. Okazawa, T. Yao, Simulation on progressive collapse behaviour of whole ship model under extreme waves using idealized structural unit method, *Mar. Struct.* 40 (2015) 104-133.
- [4] S. Tanaka, D. Yanagihara, A. Yasuoka, M. Harada, S. Okazawa, M. Fujikubo, T. Yao, Evaluation of ultimate strength of stiffened panels under longitudinal thrust, *Mar. Struct.* 36 (2014) 21-50.
- [5] M.C. Xu, Z.J. Song, J. Pan, C.G. Soares, Ultimate strength assessment of continuous stiffened panels under combined longitudinal compressive load and lateral pressure, *Ocean Eng.* 139 (2017) 39-53.

- [6] T. Xia, P. Yang, K. Hu, C. Cui, Combined effect of imperfections on ultimate strength of cracked plates under uniaxial compression, *Ocean Eng.* 150 (2018) 113-123.
- [7] M. Ozdemir, A. Ergin, D. Yanagihara, S. Tanaka, T. Yao, A new method to estimate ultimate strength of stiffened panels under longitudinal thrust based on analytical formulas, *Mar. Struct.* 59 (2018) 510-535.
- [8] W. Fricke, Fatigue analysis of welded joints: state of development, *Mar. Struct.* 16 (2003) 185-200.
- [9] S. Suresh, Fatigue of materials, 2nd *ed.*. Cambridge University Press, Cambridge, United Kingdom, 1998.
- [10] T.L. Anderson, Fracture mechanics: Fundamentals and applications, 3rd *ed.*. CRC Press, United Kingdom, 2005.
- [11] S. Tanaka, S. Okazawa, H. Okada, Y. Xi, Y. Ohtsuki, Analysis of three-dimensional surface cracks in a welded joint structure using the shell-solid mixed method, *Int. J. Offshore Polar Eng.* 23 (2013) 224-231.
- [12] R. Gadallah, N. Osawa, S. Tanaka, Evaluation of stress intensity factor for a surface cracked butt welded joint based on real welding residual stress, *Ocean Eng.* 138 (2017) 123-139.
- [13] R. Gadallah, N. Osawa, S. Tanaka, S. Tsutsumi, Critical investigation on the influence of welding heat input and welding residual stress on stress intensity factor and fatigue crack propagation, *Eng. Fail. Anal.* 89 (2018) 200-221.
- [14] R. Gadallah, N. Osawa, S. Tanaka, S. Tsutsumi, A novel approach to evaluate mixed-mode SIFs for a through-thickness crack in a welding residual stress field using an effective welding simulation method, *Eng. Fract. Mech.* 197 (2018) 48-65.
- [15] R. Gadallah, S. Tsutsumi, S. Tanaka, N. Osawa, Accurate evaluation of fracture parameters for a surface-cracked tubular T-joint taking welding residual stress into account, *Mar. Struct.* 71 (2020) 102733.

- [16] M.R. Khedmati, P. Edalat, M. Javidruzi, Sensitivity analysis of the elastic buckling of cracked plate elements under axial compression, *Thin-Walled Struct.* 47 (2009) 522-536.
- [17] S. Zhang, I. Khan, Buckling and ultimate capability of plates and stiffened panels in axial compression, *Mar. Struct.* 22 (2009) 791-808.
- [18] C.L. Yu, Y.T. Chen, S. Yang, Y. Liu, G.C. Lu, Ultimate strength characteristic and assessment of cracked stiffened panel under uniaxial compression, *Ocean Eng.* 152 (2018) 6-16.
- [19] D. Shaw, Y.H. Huang, Buckling behavior of a central cracked thin plate under tension, *Eng. Fract. Mech.* 35 (1990) 1019-1027.
- [20] E. Riks, C.C. Rankin, F.A. Bargon, Buckling behaviour of a central crack in a plate under tension, *Eng. Fract. Mech.* 43 (1992) 529-548.
- [21] G.C. Sih, Y.D. Lee, Tensile and compressive buckling of plates weakened by cracks, *Theor. Appl. Fract. Mech.* 6 (1986) 129-138.
- [22] R. Brighenti, Buckling of cracked thin-plates under tension or compression, *Thin-Walled Struct.* 43 (2005) 209-224.
- [23] R. Brighenti, Numerical buckling analysis of compressed or tensioned cracked thin plates, *Eng. Struct.* 27 (2005) 265-276.
- [24] R. Brighenti, Buckling sensitivity analysis of cracked thin plates under membrane tension or compression loading. *Nucl. Eng. Des.* 239 (2009) 965-980.
- [25] M.C. Xu, C.G. Soares, Numerical assessment of experiments on the ultimate strength of stiffened panels, *Eng. Struct.* 45 (2012) 460-471.
- [26] M.C. Xu, C.G. Soares, Experimental study on the collapse strength of wide stiffened panels, *Mar. Struct.* 30 (2013) 33-62.
- [27] M.C. Xu, Y. Garbatov, C.G. Soares, Residual ultimate strength assessment of stiffened panels with locked cracks, *Thin-Walled Struct.* 85 (2014) 398-410.

- [28] D. Yanagihara, Y. Miyake, Compressive collapse behavior of stiffened plate with cracking damage, *Conf. Proc. Jpn. Soc. Nav. Archit. Ocean Eng.* 11 (2010) 99-102. (in Japanese)
- [29] D. Yanagihara, Bending and compressive strength of stiffened panels with crack damage in longitudinal stiffeners, *Proc. of the 24th Int. Ocean Polar Eng. Conf.* (2014) 671-678.
- [30] A. Babazadeh, M.R. Khedmati, Ultimate strength of cracked ship structural elements and systems: A review, *Eng. Fail. Anal.* 89 (2018) 242-257.
- [31] S. Sadamoto, S. Tanaka, K. Taniguchi, M. Ozdemir, T.Q. Bui, C. Murakami, D. Yanagihara, Buckling analysis of stiffened plate structures by an improved meshfree flat shell formulation, *Thin-Walled Struct.* 117 (2017) 303-313.
- [32] K. Yoshida, S. Sadamoto, Y. Setoyama, S. Tanaka, T.Q. Bui, C. Murakami, D. Yanagihara, Meshfree flat-shell formulation for evaluating linear buckling loads and mode shapes of structural plates, *J. Mar. Sci. Technol.* 22 (2017) 501-512.
- [33] S. Sadamoto, M. Ozdemir, S. Tanaka, K. Taniguchi, T.T. Yu, T.Q. Bui, An effective meshfree reproducing kernel method for buckling analysis of cylindrical shells with and without cutouts, *Comput. Mech.* 59 (2017) 919-932.
- [34] M. Ozdemir, S. Tanaka, S. Sadamoto, T.T. Yu, T.Q. Bui, Numerical buckling analysis for flat and cylindrical shells including through crack employing effective reproducing kernel meshfree modeling, *Eng. Anal. Bound. Elem.* 97 (2018) 55-66.
- [35] M. Ozdemir, S. Sadamoto, S. Tanaka, S. Okazawa, T.T. Yu, T.Q. Bui, Application of 6-DOFs meshfree modeling to linear buckling analysis of stiffened plates with curvilinear surfaces, *Acta Mech.* 229 (2018) 4995-5012.
- [36] S. Tanaka, H. Suzuki, S. Sadamoto, M. Imachi, T.Q. Bui, Analysis of cracked shear deformable plates by an effective meshfree plate formulation, *Eng. Fract. Mech.* 144 (2015) 142-157.

- [37] S. Tanaka, H. Suzuki, S. Sadamoto, S. Sannomaru, T. Yu, T.Q. Bui, J-integral evaluation for 2D mixed-mode crack problems employing a meshfree stabilized conforming nodal integration method, *Comput. Mech.* 58 (2016) 185-198.
- [38] S. Tanaka, H. Suzuki, S. Sadamoto, S. Okazawa, T.T. Yu, T.Q. Bui, Accurate evaluation of mixed-mode intensity factors of cracked shear-deformable plates by an enriched meshfree Galerkin formulation, *Arch. Appl. Mech.* 87 (2017) 279-298.
- [39] S. Tanaka, M.J. Dai, S. Sadamoto, T.T. Yu, T.Q. Bui, Stress resultant intensity factors evaluation of cracked folded structures by 6DOFs flat shell meshfree modeling, *Thin-Walled Struct.* 144 (2019) 106-285.
- [40] M.J. Dai, S. Tanaka, S. Sadamoto, T.T. Yu, T.Q. Bui, Advanced reproducing kernel meshfree modeling of cracked curved shells for mixed-mode stress resultant intensity factors, *Eng. Fract. Mech.* 233 (2020) 107012.
- [41] J.K. Paik, Y.V.S. Kumar, J.M. Lee, Ultimate strength of cracked plate elements under axial compression or tension, *Thin-Walled Struct.* 43 (2005) 237-272.
- [42] J.K. Paik, Residual ultimate strength of steel plates with longitudinal cracks under axial compression-experiments, *Ocean Eng.* 35 (2008) 1775-1783.
- [43] R. Seifi, N. Khoda-yari, Experimental and numerical studies on buckling of cracked thin-plates under full and partial compression edge loading, *Thin-Walled Struct.* 49 (2011) 1504-1516.
- [44] R. Seifi, A.R. Kabiri, Lateral load effects on buckling of cracked plates under tensile loading, *Thin-Walled Struct.* 72 (2013) 37-47.
- [45] X.H. Shi, J. Zhang, C.G. Soares, Experimental study on collapse of cracked stiffened plate with initial imperfections under compression, *Thin-Walled Struct.* 114 (2017) 39-51.
- [46] S. Tanaka, S.H. Sujiatanti, Y. Setoyama, J. Yu, D. Yanagihara, Z. Pei, Buckling and collapse analysis of a cracked panel under a sequence of

tensile to compressive load employing a shell-solid mixed finite element modeling, *Eng. Fail. Anal.* 104 (2019) 987-1001.

[47] T. Murase, T. Watanabe, Study on secondary buckling behavior of thin panel, Graduation Thesis, Hiroshima University, 1997. (in Japanese)

[48] LS-DYNA, Keyword user's manual Volume I-III, 2015.